Report

Cell Reports

Structural Basis of the Diversity of Adrenergic Receptors

Graphical Abstract

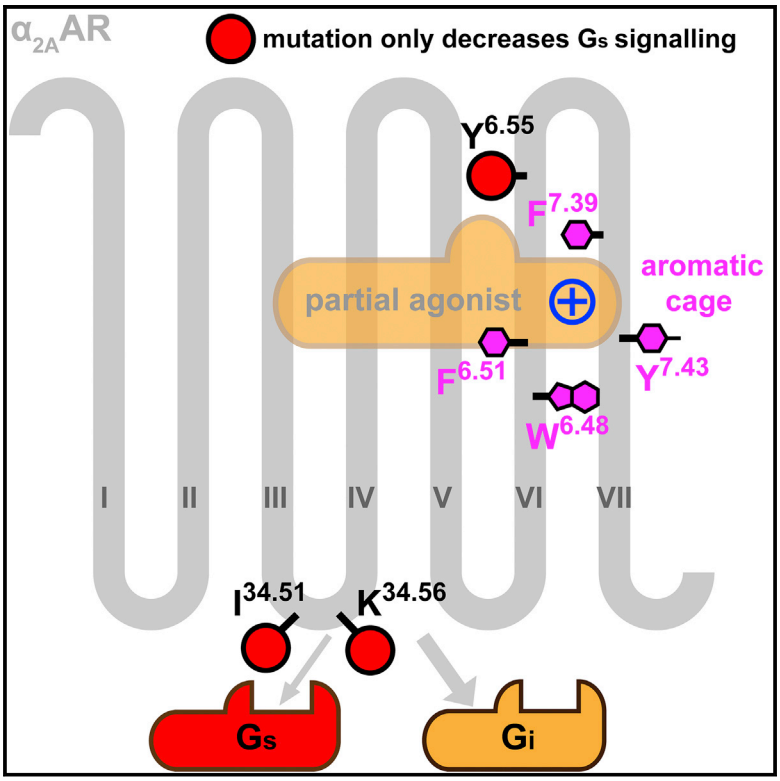

Highlights

- Partial agonist and antagonist-bound α_{2A}AR crystal structures are determined
- F412$^{7.39}$ is essential for α_{2A}AR agonist binding, sterically and energetically
- Full agonists but not partial agonists of α_{2A}AR form hbonds with Y394$^{6.55}$
- ICL2 plays key role in G_s coupling of α_{2A}AR for partial agonists

Authors

Lu Qu, Qingtong Zhou, Yueming Xu, ..., Guisheng Zhong, Dong Wu, Suwen Zhao

Correspondence

zhongsh@shanghaitech.edu.cn (G.Z.), wudong@shanghaitech.edu.cn (D.W.), zhaosw@shanghaitech.edu.cn (S.Z.)

In Brief

Crystal structures of α_{2A} adrenergic receptor (α_{2A}AR) reveal the molecular basis for the diversity in adrenergic receptors. Qu et al. define compelling roles for key amino acids in ligand binding, partial agonism, and biased signaling of α_{2A}AR.

Qu et al., 2019, Cell Reports *29*, 2929–2935
December 3, 2019
https://doi.org/10.1016/j.celrep.2019.10.088

CellPress

Cell Reports
Report

Structural Basis of the Diversity of Adrenergic Receptors

Lu Qu,[1,2,3,6] Qingtong Zhou,[1,6] Yueming Xu,[1] Yu Guo,[1,4] Xiaoyu Chen,[1,4] Deqiang Yao,[1] Gye Won Han,[5] Zhi-Jie Liu,[1,4] Raymond C. Stevens,[1,5] Guisheng Zhong,[1,4,*] Dong Wu,[1,*] and Suwen Zhao[1,4,7,*]

[1]iHuman Institute, ShanghaiTech University, Shanghai 201210, China
[2]National Laboratory of Biomacromolecules, Institute of Biophysics, Chinese Academy of Sciences, Beijing 100101, China
[3]University of Chinese Academy of Sciences, Beijing 100049, China
[4]School of Life Science and Technology, ShanghaiTech University, Shanghai 201210, China
[5]Departments of Biological Sciences and Chemistry, Bridge Institute, University of Southern California, Los Angeles, CA 90089, USA
[6]These authors contributed equally
[7]Lead Contact
*Correspondence: zhongsh@shanghaitech.edu.cn (G.Z.), wudong@shanghaitech.edu.cn (D.W.), zhaosw@shanghaitech.edu.cn (S.Z.)
https://doi.org/10.1016/j.celrep.2019.10.088

SUMMARY

Adrenergic receptors are highly homologous while at the same time display a wide diversity of ligand and G-protein binding, and understanding this diversity is key for designing selective or biased drugs for them. Here, we determine two crystal structures of the α_{2A} adrenergic receptor (α_{2A}AR) in complex with a partial agonist and an antagonist. Key non-conserved residues from the ligand-binding pocket (Phe$^{7.39}$ and Tyr$^{6.55}$) to G-protein coupling region (Ile$^{34.51}$ and Lys$^{34.56}$) are discovered to play a key role in the interplay between partial agonism and biased signaling of α_{2A}AR, which provides insights into the diversity of ligand binding and G-protein coupling preference of adrenergic receptors and lays the foundation for the discovery of next-generation drugs targeting these receptors.

INTRODUCTION

There are nine human adrenergic receptors (α_{1A}, α_{1B}, α_{1D}, α_{2A}, α_{2B}, α_{2C}, β_1, β_2, and β_3) that mediate the central and peripheral actions of catecholamines (Hein and Kobilka, 1995; Philipp and Hein, 2004a). Numerous compounds targeting adrenergic receptors, such as β-blockers, β_2 agonists, and α_2 agonists, have proven to be of therapeutic benefit in the treatment of a variety of diseases, including hypertension, angina pectoris, congestive heart failure, asthma, and depression (MacMillan et al., 1996; Philipp and Hein, 2004a; Ruffolo et al., 1993). α_{2A} Adrenergic receptor (α_{2A}AR) agonists have been used for decades in clinic for the treatment of hypertension, attention-deficit/hyperactivity disorder, and anxiety because they have sympatholytic, sedating, and analgesic effects (Ruffolo et al., 1993; Tan et al., 2002).

Although the selectivity of α_2AR is being investigated in an accompanying paper (Chen et al., 2019), we focus on understanding the structural basis of the binding and functional diversity of adrenergic receptors. More specifically, adrenergic receptors couple to different G proteins, with α_1, α_2, and β types mainly coupling to G_q, $G_{i/o}$, and G_s, respectively (Lefkowitz et al., 1988). Exceptionally, α_{2A}AR has a dual pharmacological effect in that it simultaneously couples to G_i and G_s to inhibit or stimulate adenylyl cyclase activity (Eason et al., 1992). At low agonist concentrations, α_{2A}AR mainly couples to G_i, whereas at high concentrations, G_s coupling dominates. This unusual dual effect has not been well explained for any G-protein-coupled receptor (GPCR).

Partial agonists of α_{2A}AR, such as clonidine and dexmedetomidine, tend to have better therapeutic benefits than full agonists (Philipp and Hein, 2004a; Tan et al., 2002; Vandergriff et al., 2000). The mechanism of action of these partial agonists of α_{2A}AR remain incompletely understood. Previous research on partial agonism of β_1AR and β_2AR highlight the diversified roles of three serines (S$^{5.42}$, S$^{5.43}$, and S$^{5.46}$) in transmembrane helix (TM) 5, and an asparagine (N$^{6.55}$) in TM6 played in differentiating partial agonist from full agonist (superscripts refer to Ballesteros-Weinstein numbering; Ballesteros and Weinstein, 1995; Katritch et al., 2009; Masureel et al., 2018; Warne et al., 2011). Specifically, in β_1AR, full agonists form hydrogen bonds with S$^{5.42}$ and S$^{5.46}$, but partial agonists form hydrogen bonds only with S$^{5.42}$ in a series of crystal structures. Whereas in β_2AR, different hydrogen bond networks involving S$^{5.42}$, S$^{5.43}$, N$^{6.55}$, and N$^{7.39}$ were formed upon full agonist and partial agonist binding, in crystal structures and in molecular dynamics simulations. In short, S$^{5.46}$ in β_1AR and N$^{7.39}$ in β_2AR play an essential role in differentiating partial agonist from partial agonist, respectively. The crystal structures of α_{2A}AR we solved, with partial agonist and antagonist bound, further provides the molecular basis for understanding partial agonism of GPCRs and facilitates the structure-based design of novel ligands with desired therapeutic efficacies.

RESULTS

Comparison of Two Adrenergic Receptor Structures

Two α_{2A}AR crystal structures were determined and co-crystallized with partial agonist (*S*)-4-fluoro-2-(1*H*-imidazol-5-yl)-1-isopropylindoline (RES) and antagonist (8a*R*,12a*S*,13a*S*)-12-(ethylsulfonyl)-3-methoxy-8a,12a,13a-trimethyl-6,8,8a,9,10,11,12,12a,13,13a-decahydro-5*H*-isoquinolino[2,1-g][1,6]naphthyridine (RS 79948, or in short, RS) (Figures 1, S1, and S2; Table S1). The

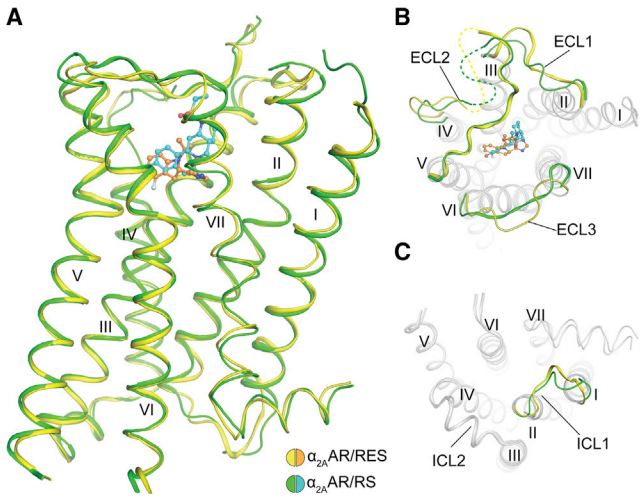

Figure 1. Crystal Structures of α_{2A}AR

(A) Overall structures of RES- (receptor in yellow and ligand in orange) and RS 79948- (receptor in green and ligand in blue) bound α_{2A}AR.

(B and C) The conformational change between the two structures at the extracellular loops (ECLs; B) and intracellular loops (ICLs; C) are shown in the colored cartoon. The disordered region in ECL2 is shown as dotted lines.

See also Tables S1 and S2 and Figures S1–S3.

former structure is in an agonist-bound inactive state and the latter is in an inactive state.

To investigate conformational changes upon agonist binding across adrenergic receptors, we compared receptors α_{2A}AR, β_1AR (Moukhametzianov et al., 2011; Warne et al., 2011), and β_2AR (Cherezov et al., 2007; Rasmussen et al., 2011; Rosenbaum et al., 2011) in the inactive, agonist-bound inactive, and active states. Remarkably, the overall structures of antagonist-bound and agonist-bound inactive states are very similar, with Cα root-mean-square deviations (RMSDs) of the α_{2A}AR (PDB: 6KUX/6KUY), β_1AR (PDB: 2YCW/2Y02), and β_2AR (PDB: 2RH1/3PDS) pairs at 1.1 Å, 0.5 Å, and 0.6 Å, respectively (Table S2). The slightly greater value of α_{2A}AR is largely due to variations in the loop regions (Figures 1B and 1C). In contrast, the overall structures of the adrenergic receptors must change significantly when forming complexes with the G protein (i.e., in fully active state), mainly due to the outward movement of the intracellular end of TM6 (Table S2).

Although the overall structures of α_{2A}AR are similar to those of βARs, obvious differences are observed in the loop region and especially extracellular ends of TM4 for receptors in the same (inactive, agonist-bound inactive, or active) state (Figure S3). Different from βARs, the extracellular end of TM4 in α_{2A}AR is unwound, which is consistent with the fact that the sequence of this region has two consecutive prolines that broke the helix. Connected to the unwound end of TM4, the starting part of ECL2 in α_{2A}AR has the typical intrinsically disordered sequence "GGGGGPQP," and indeed the electron density of this part is missing in the structure. The unwound extracellular end of TM4 and the intrinsically disordered region of ECL2 together reflect the highly dynamic nature of ECL2 in α_{2A}AR. In contrast, in βARs, the starting part of ECL2 is helical and lacks glycine or proline. Importantly, ELC2 has an extra pair of cysteines that form an intra-ECL2 disulfide bond, which further stabilizes its overall conformation. Other ECLs also have notable differences between α_{2A}AR and βARs. The unique composition and conformation of each ECL in α_{2A}AR may affect the shape and dynamics of the pocket vestibule and, as we found in the case of α_{2C}AR (Chen et al., 2019), may have an impact on ligand selectivity.

The Ligand-Binding Diversity of Adrenergic Receptors

Electron densities for RES and RS 79948 in the two structures of α_{2A}AR enable us to convincingly make the placement of the two ligands (Figure S1). The two ligands show strong interactions with residues in the pocket of α_{2A}AR, both including a salt bridge between the ligand's positively charged nitrogen atom and $D113^{3.32}$—the conserved residue involved in ligand binding in all aminergic receptors and opioid receptors (Figures 2A–2D). The binding pocket of α_{2A}AR is composed of 12 residues (Figure S4). Although the backbone conformations of the pocket-forming residues are rather similar in the two α_{2A}AR structures, the shapes of the two binding pockets are strikingly different due to the repacking of four sidechains ($F412^{7.39}$, $Y416^{7.43}$, $Y394^{6.55}$, and $D113^{3.32}$) upon binding with different ligands (Figures 2C, 2E, and S4A–S4D). These dramatic sidechain rearrangements reflect the highly plastic nature of the receptor to accommodate ligands with very different chemical scaffolds, such as RES and RS 79948 (Figures 2A and 2B).

Interestingly, when we tried to dock agonists and antagonists of α_{2A}AR into the two structures, we found that agonists (especially when containing an imidazole ring head like RES) fit better in the RES-bound structure (i.e., agonist-bound inactive state), whereas antagonists fit better in the RS-bound structure (i.e., inactive state) (Table S3). This finding implies that the shapes of the pockets of the two structures are specific to the agonists and antagonists of this receptor. Conversely, in βAR, generally agonists can be docked into the pocket of antagonist-bound structures, and vice versa, which reflects the relative rigidity of the binding pocket of βAR (Beuming and Sherman, 2012).

$F412^{7.39}$ Is Essential for α_{2A}AR Agonist Binding as a Switching Lid of an Aromatic Cage

Among these conformational rearranged residues, the most intriguing is $F412^{7.39}$, which functions as a switching lid for the pocket. Large ligands, like RS 79948 with a saturated ring system, push $F412^{7.39}$ aside, making the pocket large and open. Conversely, small ligands, like RES, can induce the closure of the lid (i.e., $F412^{7.39}$) to form an aromatic cage together with residues $W387^{6.48}$, $F390^{6.51}$, and $Y416^{7.43}$ (Figure S4E). By forming the aromatic cage around the cation in the ligand not only is the steric of the site tightly defined but also the energetics. Notably, the residue at 7.39 is one of the three non-conserved residues (the other two are 6.55 and 5.43) (Figure S5) in the binding pocket of adrenergic receptors (Figures 2C and 2D; Table S4). Thus, the "switching lid" phenomenon seems unique to αARs. In fact, even among aminergic and opioid receptors, only αARs, muscarinic receptors, and two histamine receptors (H3 and H4) have aromatic residues at the four positions 6.48, 6.51, 7.39, and 7.43 (Table S4). Unlike α_{2A}AR, in muscarinic receptors, there is no dramatic repacking of $Y^{7.39}$ upon agonist binding; thus, $Y^{7.39}$ forms a rather static cage restricting the

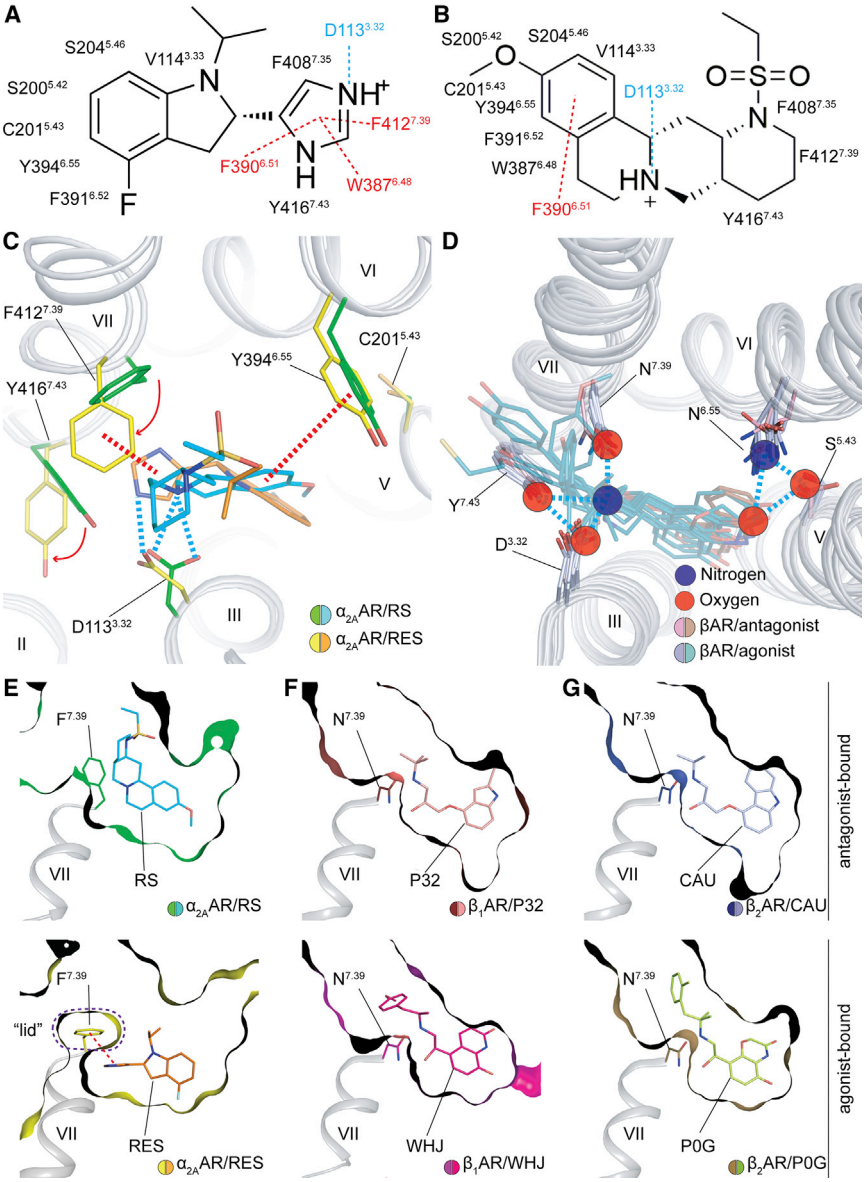

Figure 2. Binding Pocket Analysis of Adrenergic Receptors

(A and B) Schematic representation of RES (A) and RS 79948 (B) contacts with α_{2A}AR. Here and subsequently, dotted lines indicate interaction types: blue for salt bridge or hydrogen bond and red for π-π interactions.

(C) Top view of α_{2A}AR-RES complex (receptor in yellow, ligand in blue) and α_{2A}AR-RS complex model (receptor in green, ligand in orange) binding pocket. Conformational changes are illustrated by red arrows. Large side chain conformational changes were observed at F412 and Y416.

(D) Critical interactions in binding pockets of βARs with antagonist-bound structures in pink and agonist in light blue. Hydrogen donors are shown as blue dots and receivers as red dots. The hydrogen network between ligands and $N^{6.55}$ exist only in agonist-bound structures. β_1AR-antagonist, PDB: 2YCW; β_2AR-antagonist, PDB: 2RH1; β_1AR-agonist, PDB: 2Y00, 2Y01, 2Y02, 2Y03, and 2Y04; β_2AR-agonist, PDB: 3SN6, 4LDO, 4LDL, and 4QKX.

(E–G) The reshaping of binding pockets in α_{2A}AR (6KUX/6KUY) (E), β_1AR (4BVN/2Y02) (F), and β_2AR (2RH1/4LDE) (G).

See also Tables S3–S5 and Figures S4–S7.

muscarinic ligands while isolating the allosteric modulator from the ligand-binding pocket (Figures S4E and S4F). Such a rigid or flexible aromatic cage plays a substantial role in cation recognition in these receptors. Thus, it has particular implications for ligand discovery.

This aromatic cage was not observed in βARs (Figures 2F and 2G) where the residue at 7.39 is a much smaller asparagine and shows no obvious conformational changes during various ligand binding because $N^{7.39}$ is involved in a stable hydrogen bond with the conserved positively charged ligand nitrogen (Figure 2D). Interestingly, the $F412^{7.39}N$ mutation in α_{2A}AR (i.e., mutation to the residue at 7.39 in βARs) abolished the function of all four partial and full agonists we tested (clonidine, guanabenz, UK14,304, and epinephrine), reflecting the essential π-π and cation-π interactions provided by $F412^{7.39}$ for the activity of α_{2A}AR agonists (Figure S6A). Similarly, the $F312^{7.39}$A/L mutation in α_{1A}AR also abolishes the binding of ligands containing an imidazoline ring (Waugh et al., 2001), which is indicative of the critical function of the phenylalanine at 7.39 for αARs. Interestingly, the $F412^{7.39}N$ mutation in α_{2A}AR has no response to two β_2AR selective agonists, namely salmenterol and salbutamol (Figure S6A), implying the other two non-conserved residues ($Y394^{6.55}$ and $C201^{5.43}$) in the binding pocket also play important roles in ligand activity. Nevertheless, $F412^{7.39}N$ and $Y394^{6.55}N/F412^{7.39}N$ abolish the activation activity of α_{2A}AR agonists and partial agonists, possibly due to the key role $F412^{7.39}$ plays in agonist binding; yet, they are still unable to trigger the activity of β_2AR ligands x(Figures S6). This finding implies that other regions, such as ECLs, may also be important for the binding and function of β_2AR ligands.

Full but Not Partial Agonists Form Hydrogen Bonds with $Y394^{6.55}$ and $S200^{5.42}/S204^{5.46}$

In both α_{2A}AR structures, $Y394^{6.55}$, another non-conserved position in the ligand-binding pocket of adrenergic receptors, has no direct interaction with ligands, whereas in β_2AR, $N^{6.55}$ forms a strong and conserved hydrogen bond with full agonist but not partial agonist (Figure 2D) (Masureel et al., 2018). In fact, hydrogen bond formation between $N^{6.55}$ and $S^{5.43}$ is believed to be a hallmark of the activation of βARs (Masureel et al., 2018). As a result, the role of $Y394^{6.55}$ in α_{2A}AR is particularly intriguing. From the RES-bound structure, we knew that

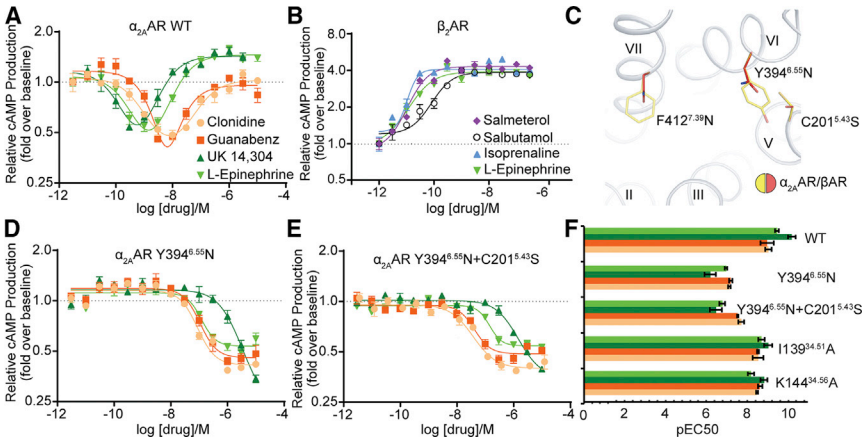

Figure 3. Y394$^{6.55}$ Plays a Key Role in Biased Signaling of α_{2A}AR

(A) The dual effect of WT α_{2A}AR in CHO cells.

(B) Unlike α_{2A}AR, agonists and antagonists of β_2AR show only G_s activity.

(C) Positions of the mutations used for functional assays.

(D) Mutation of Y394$^{6.55}$N abolished the G_s signal in α_{2A}AR.

(E) The double mutation of Y394$^{6.55}$N and C201$^{5.43}$S kept the effect of Y394$^{6.55}$N.

(F) The pEC_{50} (i.e., $-lgEC_{50}$) values of the G_i pathway in the cyclic AMP (cAMP) assay of α_{2A}AR WT and mutants. Data are represented as mean ± SEM of $n \geq 3$ independent experiments. See also Figure S5.

the partial agonist RES has no interaction with Y394$^{6.55}$. We further checked the docking poses of representative full agonists (epinephrine, norepinephrine, and UK14,304) and partial agonists (clonidine, guanfacine, guanabenz, and dexmedetomidine) to see if Y394$^{6.55}$ contributes to partial agonism in α_{2A}AR as N$^{6.55}$ does in β_2AR. The docking results show that all three full agonists of α_{2A}AR formed hydrogen bonds with Y394$^{6.55}$ and S200$^{5.42}$/S204$^{5.46}$, but all partial agonists do not (Figure S7). The reason is that the tails of partial agonists generally are more hydrophobic, whereas tails of full agonists are more hydrophilic and, thus, are prone to hydrogen bond forming (Figures S7 and S8). Because the movements of the extracellular end (which participates in ligand binding) and the intracellular end of TM6 (which interacts with the G protein) are more or less coupled, the strong interaction between full agonists and the extracellular end of TM6 could, in turn, push TM6 to be more kinked, which leads to more outward movement of the intracellular end of TM6 (i.e., more activated). In contrast, partial agonists can only form weaker interactions with TM6, which will lead to less outward movement of intracellular end of TM6 (i.e., less activated).

Notably, the roles of residues at positions 6.55, 5.42, and 5.46 in differentiating full agonist from partial agonist are diverse in adrenergic receptors. In α_{2A}AR and β_2AR, full agonists form a hydrogen bond with 6.55 but partial agonists do not, although position 6.55 is not conversed in the two receptors (Table S5). In β_1AR, full agonists form a hydrogen bond with S$^{5.46}$ but partial agonists do not (Warne et al., 2011), while in α_{2A}AR, full agonists cannot reach S$^{5.46}$ (Table S5).

Role of Non-conversed Residues in Dual Coupling of α_{2A}AR to Two G Proteins

The movement of the intracellular end of TM6 is the hallmark of GPCR activation. Recent electron microscopy (EM) structures of GPCR-G_i complexes revealed that TM6 are less kinked compared to those in GPCR-G_s complexes (Draper-Joyce et al., 2018; García-Nafría et al., 2018; Kang et al., 2018; Koehl et al., 2018). Thus, we hypothesized that TM6 of α_{2A}AR is in two different states when the receptor couples to different G proteins. Using functional studies of α_{2A}AR mutants, we investigated the role of the two non-conserved residues Y394$^{6.55}$and C201$^{5.43}$ in dual coupling of α_{2A}AR to G_i and G_s by mutating them to residues in β_2AR.

Consistent with previous reports, wild-type (WT) α_{2A}AR simultaneously coupled to both G_i and G_s proteins (termed "dual effect"; Eason et al., 1992) when stimulated by full agonist adrenaline, UK14,304, or partial agonists clonidine and guanabenz (Figure 3A). Conversely, full or partial agonists of β_2AR could only activate the G_s signal (Figure 3B). We hypothesized that the non-conserved residues in the pocket may cause this dual effect. Therefore, we designed mutations to minimize the dual effect of α_{2A}AR. Surprisingly, with the single mutation Y394$^{6.55}$N, the dual effect disappeared (Figures 3C and 3D), and the same result was achieved when adding another mutation: C201$^{5.43}$S (Figure 3E). Both mutations caused an approximately 10-fold half maximal effective concentration (EC_{50}) loss (Figure 3F). These results confirm the key role Y394$^{6.55}$ plays in G-protein selectivity of α_{2A}AR.

G Protein Binding Site Diversity in Adrenergic Receptors

The activation of G protein is affected not only by the ligand-binding pocket but also by the G protein binding site. One region that may impact the G protein binding preference is ICL2, which often has more contacts with G_s than G_i (Figure 4A). Based on structural analysis of the β_2AR-G_s complex (PDB: 3SN6[21]), we predicted that I$^{34.51}$ would form intensive hydrophobic interactions with H41 and F376 in G_s (Figure 4B). Similarly, residue K144$^{34.56}$ would form electrostatic interactions with D139 in G_s. As a result, two mutations, namely, I139$^{34.51}$A and K144$^{34.56}$A, were designed to see if they would hamper the coupling of G_s when the receptor binds with full or partial agonists. To evaluate the G_s signaling without the interference of G_i signaling, pertussis toxin (PTX), which can selectively block the G_i signaling pathway, was introduced. With PTX, we can see that WT α_{2A}AR has strong G_s signaling for full agonists and rather weak G_s signaling for partial agonists (Figure 4C). The I139$^{34.51}$A mutant can abolish G_s signaling for both partial agonists and full agonists (Figure 4D). Unlike I139$^{34.51}$A, K144$^{34.56}$A could selectively diminish the G_s potency of partial agonists clonidine and guanabenz, leaving the G_s potency of full agonists

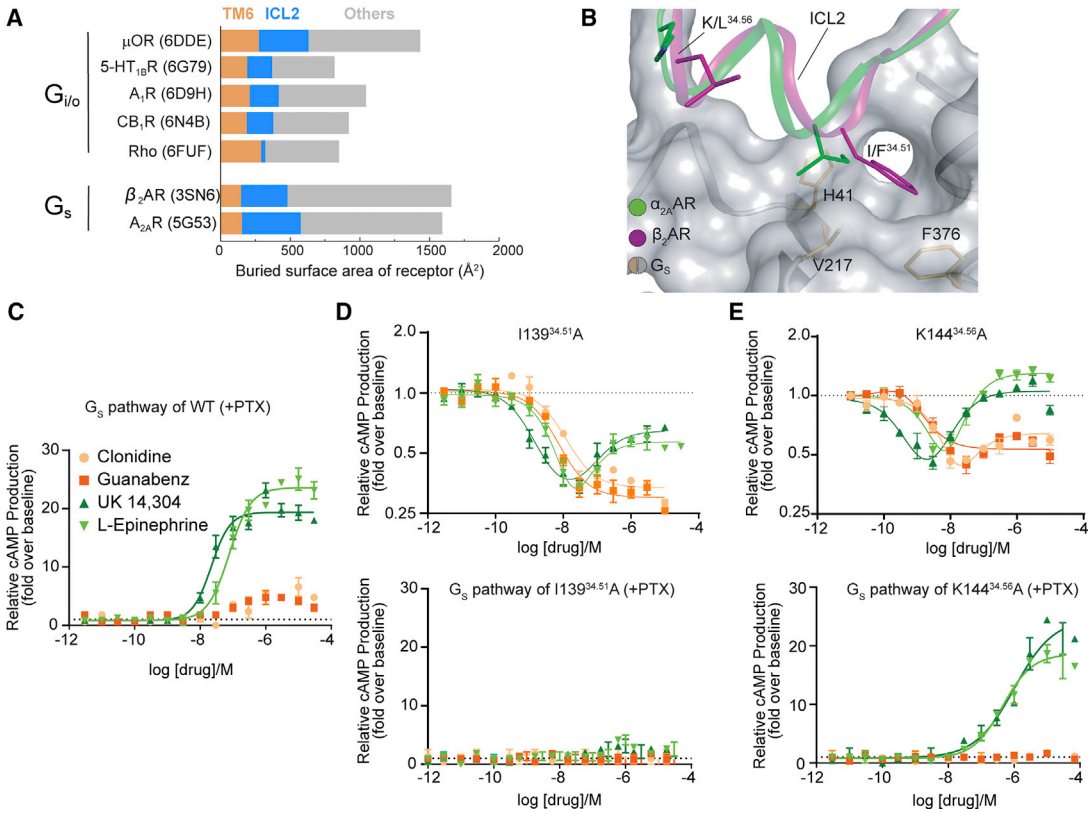

Figure 4. ICL2 Plays Essential Role in G_s Coupling for Partial Agonists of α_{2A}AR

(A) Buried surface area of receptors in GPCR-G protein complexes. TM6 has more buried surface in G_i-coupled complexes, whereas ICL2 usually has less contacts with G_i than G_s.

(B) AR-G_s interface around ICL2, with the structure of α_{2A}AR aligned to that of G_s-bound β_2AR. $I^{34.51}$ and $K^{34.56}$ in α_{2A}AR are two residues that may interact with G_s.

(C–E) α_{2A}AR G_s signaling when treated by PTX.

(C) WT α_{2A}AR has strong G_s signaling for full agonists and weak G_s signaling for partial agonists.

(D) $I139^{34.51}A$ mutation does not affect G_i signaling of α_{2A}AR, but it completely abolishes G_s signaling for both agonists and partial agonists.

(E) $K144^{34.56}A$ mutant abolishes G_s signaling for partial agonists but does not affect the G_s coupling of full agonist too much. Data are represented as mean ± SEM of n ≥ 3 independent experiments.

See also Figures S7 and S8.

UK14,304 and epinephrine less affected (Figure 4E). Notably, the G_i potencies of $I139^{34.51}A$ and $K144^{34.56}A$ mutants were more or less similar to that of WT α_{2A}AR for both partial and full agonists (Figures 4D, 4E, and 3F).

The distinct pharmacological consequence of the two mutants ($I139^{34.51}A$ and $K144^{34.56}A$) for partial and full agonists sheds light on the interplay between partial agonism and biased signaling of α_{2A}AR. Both mutants completely abolished the weak G_s signaling for partial agonists, and they convert partial agonists clonidine and guanabenz to G_i-biased agonists from the perspective of pharmacology. Unlike full agonists, partial agonists of α_{2A}AR lack of hydrophilic tails (Figure S8) that can form hydrogen bonds with polar residues ($Y^{6.55}$, $S^{5.42}$ or $S^{5.46}$) in the extracellular end of TM5 and TM6 (Figure S7); thus, it is difficult for them to promote the outward movement of the intracellular end of TM6 as large as that required for G_s coupling. The two mutations on ICL2 push the energy barrier for G_s coupling induced by partial agonists even higher, and they become the last straw. On the other hand, full agonists can form strong interactions with the extracellular end of TM5 and TM6 (Figure S7); thus, they may push the receptor to have a higher population in the G_s-coupling state. The G_s signaling pathway of α_{2A}AR induced by full agonists was largely unaffected by $K144^{34.56}A$ but was nearly abolished by $I139^{34.51}A$. The difference highlights the curial role of $I139^{34.51}$ on G_s coupling, and it infers that the $I139^{34.51}A$ mutant may lose the G_s coupling ability. Taken together, these results demonstrate the essential role of ICL2 in G_s coupling for partial agonists and reflects the allosteric communication between extracellular ligand binding and intracellular G protein coupling.

DISCUSSION

Our comparative study of two α_{2A}AR crystal structures in binding poses with very different ligands has identified key non-conserved residues from the ligand binding pocket ($F412^{7.39}$ and $Y394^{6.55}$) to the G protein coupling region ($I139^{34.51}$, $K144^{34.56}$) that control adrenergic diversity through ligand

binding, partial agonism, and G protein preference. Remarkably, we found that G protein signaling can be dramatically altered or even abolished by several single mutations, revealing how evolution has been able to achieve the diversity of adrenergic receptor function with minimal modifications. Together with accompanying insights on adrenergic selectivity (Chen et al., 2019), our results will lay the foundation for next-generation drug discovery efforts targeting adrenergic receptors.

STAR★METHODS

Detailed methods are provided in the online version of this paper and include the following:

- KEY RESOURCES TABLE
- LEAD CONTACT AND MATERIALS AVAILABILITY
- EXPERIMENTAL MODEL AND SUBJECT DETAILS
  - Cell lines
- METHOD DETAILS
  - Protein Engineering for Structure Determination
  - Protein Expression
  - Protein Purification
  - Lipidic Cubic Phase Crystallization
  - Data Collection and Structure Determination
  - Cell culture and transfection for cAMP assay
  - Split luciferase biosensor cAMP assay
  - Ligand docking
- QUANTIFICATION AND STATISTICAL ANALYSIS
- DATA AND CODE AVAILABILITY

SUPPLEMENTAL INFORMATION

Supplemental Information can be found online at https://doi.org/10.1016/j.celrep.2019.10.088.

ACKNOWLEDGMENTS

This work was supported by National Natural Science Foundation of China 31971178 (S.Z.), 31771130 (G.Z.), and 21704064 (Q.Z.); National Key R & D Program of China grants 2016YFC0905900 (S.Z. and G.Z.), 2018YFA0507000 (S.Z.), and 2017YFC1001300 (G.Z.); the 2015 Thousand Youth Talents Plan of China (G.Z.); and ShanghaiTech University, China. We thank Sanofi for providing the compound RES. The diffraction data were collected at GM/CA@APS of Argonne National Laboratory, X06SA@SLS of the Paul Scherrer Institute, and BL41XU@ Spring-8. We would also like to thank: M. Wang, C.-Y. Huang, V. Olieric, K. Hasegawa, N. Mizuno, T. Kawamura, and H. Murakami for help with data collection; S. Zaidi and V. Katritch for support on structure and docking analysis; B.L. Roth and J.D. McCorvy for help on cell assay; the Cloning core, BV core, and Purification core of iHuman for help in clones, protein expression, and material supply; M.A. Hanson and L. Wu for help with data processing; and Q. Sun for help with protein purification.

AUTHOR CONTRIBUTIONS

L.Q., construct design, crystallization, data collection and processing, structure determination and refinement, data analysis; D.W., cloning, construct design, data collection; Y.X. and X.C., functional studies; Y.G., docking; D.Y. and G.W.H., data processing and structure refinement; R.C.S. and Z.-J.L., structure analysis; Q.Z., D.W., G.Z., and S.Z., project design and supervision; L.Q., Q.Z., G.Z., and S.Z., manuscript writing with input from the other authors.

DECLARATION OF INTERESTS

The authors have declared that no competing interests exist.

Received: June 18, 2019
Revised: September 23, 2019
Accepted: October 22, 2019
Published: December 3, 2019

REFERENCES

Abraham, M.J., Murtola, T., Schulz, R., Páll, S., Smith, J.C., Hess, B., and Lindahl, E. (2015). GROMACS: High performance molecular simulations through multi-level parallelism from laptops to supercomputers. SoftwareX *1–2*, 19–25.

Adams, P.D., Afonine, P.V., Bunkóczi, G., Chen, V.B., Davis, I.W., Echols, N., Headd, J.J., Hung, L.W., Kapral, G.J., Grosse-Kunstleve, R.W., et al. (2010). PHENIX: a comprehensive Python-based system for macromolecular structure solution. Acta Crystallogr. D Biol. Crystallogr. *66*, 213–221.

Ballesteros, J.A., and Weinstein, H. (1995). Integrated methods for the construction of three-dimensional models and computational probing of structure-function relations in Gprotein-coupled receptors. In Methods in Neurosciences, C.S. Stuart, ed. (Academic Press), pp. 366–428.

Beuming, T., and Sherman, W. (2012). Current assessment of docking into GPCR crystal structures and homology models: successes, challenges, and guidelines. J. Chem. Inf. Model. *52*, 3263–3277.

Cherezov, V., Rosenbaum, D.M., Hanson, M.A., Rasmussen, S.G., Thian, F.S., Kobilka, T.S., Choi, H.J., Kuhn, P., Weis, W.I., Kobilka, B.K., and Stevens, R.C. (2007). High-resolution crystal structure of an engineered human beta2-adrenergic G protein-coupled receptor. Science *318*, 1258–1265.

Chen, X., Xu, Y., Qu, L., Wu, L., Han, G.W., Guo, Y., Wu, Y., Zhou, Q., Sun, Q., Yang, J., et al. (2019). Molecular mechanism for ligand recognition and subtype selectivity of α2c adrenergic receptors. Cell Rep *27*, Published online December 3, 2019. https://doi.org/10.1016/j.celrep.2019.10.112.

Cherezov, V., Hanson, M.A., Griffith, M.T., Hilgart, M.C., Sanishvili, R., Nagarajan, V., Stepanov, S., Fischetti, R.F., Kuhn, P., and Stevens, R.C. (2009). Rastering strategy for screening and centring of microcrystal samples of human membrane proteins with a sub-10 microm size X-ray synchrotron beam. J. R. Soc. Interface *6* (*Suppl 5*), S587–S597.

Collaborative Computational Project, Number 4. (1994). The CCP4 suite: programs for protein crystallography. Acta Crystallogr. D Biol. Crystallogr. *50*, 760–763.

Draper-Joyce, C.J., Khoshouei, M., Thal, D.M., Liang, Y.L., Nguyen, A.T.N., Furness, S.G.B., Venugopal, H., Baltos, J.A., Plitzko, J.M., Danev, R., et al. (2018). Structure of the adenosine-bound human adenosine A_1 receptor-G_i complex. Nature *558*, 559–563.

Eason, M.G., Kurose, H., Holt, B.D., Raymond, J.R., and Liggett, S.B. (1992). Simultaneous coupling of alpha 2-adrenergic receptors to two G-proteins with opposing effects. Subtype-selective coupling of alpha 2C10, alpha 2C4, and alpha 2C2 adrenergic receptors to Gi and Gs. J. Biol. Chem. *267*, 15795–15801.

Emsley, P., Lohkamp, B., Scott, W.G., and Cowtan, K. (2010). Features and development of Coot. Acta Crystallogr. D Biol. Crystallogr. *66*, 486–501.

Friesner, R.A., Banks, J.L., Murphy, R.B., Halgren, T.A., Klicic, J.J., Mainz, D.T., Repasky, M.P., Knoll, E.H., Shelley, M., Perry, J.K., et al. (2004). Glide: a new approach for rapid, accurate docking and scoring. 1. Method and assessment of docking accuracy. J. Med. Chem. *47*, 1739–1749.

Friesner, R.A., Murphy, R.B., Repasky, M.P., Frye, L.L., Greenwood, J.R., Halgren, T.A., Sanschagrin, P.C., and Mainz, D.T. (2006). Extra precision glide: docking and scoring incorporating a model of hydrophobic enclosure for protein-ligand complexes. J. Med. Chem. *49*, 6177–6196.

García-Nafría, J., Nehmé, R., Edwards, P.C., and Tate, C.G. (2018). Cryo-EM structure of the serotonin 5-HT_{1B} receptor coupled to heterotrimeric G_o. Nature *558*, 620–623.

Hein, L., and Kobilka, B.K. (1995). Adrenergic receptor signal transduction and regulation. Neuropharmacology *34*, 357–366.

Kabsch, W. (2010). XDS. Acta Crystallogr. D Biol. Crystallogr. *66*, 125–132.

Kang, Y., Kuybeda, O., de Waal, P.W., Mukherjee, S., Van Eps, N., Dutka, P., Zhou, X.E., Bartesaghi, A., Erramilli, S., Morizumi, T., et al. (2018). Cryo-EM structure of human rhodopsin bound to an inhibitory G protein. Nature *558*, 553–558.

Katritch, V., Reynolds, K.A., Cherezov, V., Hanson, M.A., Roth, C.B., Yeager, M., and Abagyan, R. (2009). Analysis of full and partial agonists binding to beta2-adrenergic receptor suggests a role of transmembrane helix V in agonist-specific conformational changes. J. Mol. Recognit. *22*, 307–318.

Koehl, A., Hu, H., Maeda, S., Zhang, Y., Qu, Q., Paggi, J.M., Latorraca, N.R., Hilger, D., Dawson, R., Matile, H., et al. (2018). Structure of the μ-opioid receptor-G_i protein complex. Nature *558*, 547–552.

Lefkowitz, R.J., Kobilka, B.K., Benovic, J.L., Bouvier, M., Cotecchia, S., Hausdorff, W.P., Dohlman, H.G., Regan, J.W., and Caron, M.G. (1988). Molecular biology of adrenergic receptors. Cold Spring Harb. Symp. Quant. Biol. *53*, 507–514.

MacMillan, L.B., Hein, L., Smith, M.S., Piascik, M.T., and Limbird, L.E. (1996). Central hypotensive effects of the alpha2a-adrenergic receptor subtype. Science *273*, 801–803.

Masureel, M., Zou, Y., Picard, L.P., van der Westhuizen, E., Mahoney, J.P., Rodrigues, J.P.G.L.M., Mildorf, T.J., Dror, R.O., Shaw, D.E., Bouvier, M., et al. (2018). Structural insights into binding specificity, efficacy and bias of a β_2AR partial agonist. Nat. Chem. Biol. *14*, 1059–1066.

McCoy, A.J., Grosse-Kunstleve, R.W., Adams, P.D., Winn, M.D., Storoni, L.C., and Reada, R.J. (2007). Phaser crystallographic software. Journal of Applied Crystallography *40*, 658–674.

Moukhametzianov, R., Warne, T., Edwards, P.C., Serrano-Vega, M.J., Leslie, A.G., Tate, C.G., and Schertler, G.F. (2011). Two distinct conformations of helix 6 observed in antagonist-bound structures of a beta1-adrenergic receptor. Proc. Natl. Acad. Sci. USA *108*, 8228–8232.

Philipp, M., and Hein, L. (2004a). Adrenergic receptor knockout mice: distinct functions of 9 receptor subtypes. Pharmacol. Ther. *101*, 65–74.

Rasmussen, S.G., DeVree, B.T., Zou, Y., Kruse, A.C., Chung, K.Y., Kobilka, T.S., Thian, F.S., Chae, P.S., Pardon, E., Calinski, D., et al. (2011). Crystal structure of the β2 adrenergic receptor-Gs protein complex. Nature *477*, 549–555.

Rosenbaum, D.M., Zhang, C., Lyons, J.A., Holl, R., Aragao, D., Arlow, D.H., Rasmussen, S.G., Choi, H.J., Devree, B.T., Sunahara, R.K., et al. (2011). Structure and function of an irreversible agonist-β(2) adrenoceptor complex. Nature *469*, 236–240.

Ruffolo, R.R., Jr., Nichols, A.J., Stadel, J.M., and Hieble, J.P. (1993). Pharmacologic and therapeutic applications of alpha 2-adrenoceptor subtypes. Annu. Rev. Pharmacol. Toxicol. *33*, 243–279.

Smart, O.S., Womack, T.O., Flensburg, C., Keller, P., Paciorek, W., Sharff, A., Vonrhein, C., and Bricogne, G. (2012). Exploiting structure similarity in refinement: automated NCS and target-structure restraints in BUSTER. Acta Crystallogr. D Biol. Crystallogr. *68*, 368–380.

Tan, C.M., Wilson, M.H., MacMillan, L.B., Kobilka, B.K., and Limbird, L.E. (2002). Heterozygous alpha 2A-adrenergic receptor mice unveil unique therapeutic benefits of partial agonists. Proc. Natl. Acad. Sci. USA *99*, 12471–12476.

Vandergriff, J., Kallman, M.J., and Rasmussen, K. (2000). Moxonidine, a selective imidazoline-1 receptor agonist, suppresses the effects of ethanol withdrawal on the acoustic startle response in rats. Biol. Psychiatry *47*, 874–879.

Warne, T., Moukhametzianov, R., Baker, J.G., Nehmé, R., Edwards, P.C., Leslie, A.G., Schertler, G.F., and Tate, C.G. (2011). The structural basis for agonist and partial agonist action on a β(1)-adrenergic receptor. Nature *469*, 241–244.

Waugh, D.J., Gaivin, R.J., Zuscik, M.J., Gonzalez-Cabrera, P., Ross, S.A., Yun, J., and Perez, D.M. (2001). Phe-308 and Phe-312 in transmembrane domain 7 are major sites of alpha 1-adrenergic receptor antagonist binding. Imidazoline agonists bind like antagonists. J. Biol. Chem. *276*, 25366–25371.

Zoete, V., Cuendet, M.A., Grosdidier, A., and Michielin, O. (2011). SwissParam: A fast force field generation tool for small organic molecules. Journal of Computational Chemistry *32*, 2359–2368.

STAR★METHODS

KEY RESOURCES TABLE

REAGENT or RESOURCE	SOURCE	IDENTIFIER
Chemicals, Peptides, and Recombinant Proteins		
EDTA-free complete protease inhibitor cocktail tablets	Roche	Cat#5056489001
Iodoacetamide	Sigma	Cat#I1149
n-dodecyl-beta-D-maltoside (DDM)	Anatrace	Cat#4216588
Cholesterol hemisucinate (CHS)	Sigma	Cat#C6512
N-[4-(7-diethylamino-4-methyl-3-coumarinyl)phenyl] maleimide (CPM)	Invitrogen	Cat#D10251
TALON IMAC resin	Clontech	Cat#635507
1-Oleoyl-rac-glycerol (monoolein)	Sigma	Cat#M7765
Cholesterol	Sigma	Cat#C8667
RS 79948	Tocris	Cat#0987/50
RES	GPCR consortium	N/A
Clonidine	Medchemexpress	Cat#HY-B0409A
Guanabenz	Medchemexpress	Cat# HY-B0566
UK14,304	Medchemexpress	Cat#HY-B0659A
L-Epinephrine	Medchemexpress	Cat#HY-B0447B
Salmeterol	Medchemexpress	Cat# HY-14302
Salbutamol	Medchemexpress	Cat#HY-B0436
Isoprenaline	Medchemexpress	Cat# HY-B0468
Critical Commercial Assays		
HTRF HiRange cAMP Assay Kit	CISBIO	Cat# 62AM6PEC
PathHunter Detection Kit	DiscoveRx	Cat#93-0001
Q5 site directed mutagenesis kit	NEB	Cat#E0554S
In-Fusion® HD EcoDry™ Cloning System	Clontech	Cat#639684
Deposited Data		
α_{2A}AR-RS 79948 complex structure	This paper	PDB: 6KUX
α_{2A}AR-RES complex structure	This paper	PDB: 6KUY
Experimental Models: Cell Lines		
Spodoptera frugiperda (Sf9)	A gift from Dr. Beili Wu (SIMM, CAS)	N/A
HEK293T	ATCC	Cat#CCL-3216
Phoenix-AMPHO	Allele Biotechnology	Cat#ABP-RCV-10001
CHO-K1	ATCC	Cat#CCL-61
PathHunter® U2OS EA β-Arrestin Parental Cell Line	DiscoveRx	Cat#93-0166
CHO-hCB1R PathHunter DiscoveRx	DiscoveRx	Cat#93-0959C2
Oligonucleotides		
Primers for cloning α_{2A}AR-WT into pcDNA 3.1 (+) vector (Table S6)		N/A
Primers for site-direct mutagenesis (Table S6)		N/A
Recombinant DNA		
pcDNA 3.1 (+) vector	Thermo Scientific	V79020
Software and Algorithms		
Schrödinger Suite 2018-3	Schrödinger	https://www.schrodinger.com
GROMACS 5.1.2	Abraham et al., 2015	http://www.gromacs.org
SwissParam	Zoete et al., 2011	http://www.swissparam.ch

(*Continued on next page*)

Continued

REAGENT or RESOURCE	SOURCE	IDENTIFIER
XDS	Kabsch, 2010	http://Xds.mpimf-heidelberg.mpg.de
SCALA	Collaborative Computational Project, Number 4, 1994	http://www.ccp4.ac.uk/html/scala.html
Phaser	McCoy et al., 2007	http://www.phenix-online.org
Phenix	Adams et al., 2010	http://www.phenix-online.org
Buster	Smart et al., 2012	http://www.globalphasing.com/buster
COOT	Emsley et al., 2010	https://www2.mrc-lmb.cam.ac.uk/personal/pemsley/coot
Prism v.7.0	GraphPad Software Inc.	N/A
FlowJo® v.10.5.0	FlowJo, LLC	https://www.flowjo.com/solutions/flowjo
FluoView FV1000	Olympus - Life Science Solutions	https://www.olympus-lifescience.com/en/
Other		
Solid white 384-well assay plates	VWR	Cat#82051-278 (CS)
Low-volume (20 μL) 384-well assay plates	VWR	Cat#784080
DMEM/F-12 (1:1) cell culture media	Invitrogen	Cat#11330-057
Opti-MEM cell culture media	Invitrogen	Cat#11058-021
FreeStyle™ 293 Expression Medium	Life Technologies	Cat#12338-026
DMEM	Invitrogen	Cat#11965-118
MEM	Invitrogen	Cat#11095-098
Pertussis Toxin	Tocris	Cat#3097
Phoenix package system	Stanford University	N/A
Penicillin/Streptomycin	Invitrogen	Cat#15140-122
Puromycin	Invitrogen	Cat#A11138-03
Hygromycin B	Life Technologies	Cat#10687-010
Geneticin	Life Technologies	Cat#10131-035
Bovine Serum Albumin, Fraction V, Cold-ethanol Precipitated	Fisher Scientific	Cat#BP1605100
Trypsin 0.5% EDTA	Invitrogen	Cat#25300-120
Dulbecco's phosphate-buffered saline (DPBS)	Invitrogen	Cat#14190250
4',6-Diamidino-2-phenylindole dihydrochloride (DAPI)	Sigma	Cat#D8417
Fetal Bovine Serum (FBS)	Life Technologies	Cat#16140089
Ethylenediamine Tetraacetic Acid (EDTA)	Fisher Scientific	Cat#S311-500
Glass bottom dishes-uncoated (confocal plates)	MatTek	Cat#P35G-10-14-C
Collagen I	Fisher	Cat#CB40231
100kDa cutoff concentrators	Sartorius	Cat#VS0642
PD Minitrap G-25 coulmn	GE Healthcare	Cat#28-9180-07
96-well glass sandwich plates for LCP crystallization	NOVA	Cat#NOA90020
Lipofectamine® 2000	Thermo Scientific	11668027

LEAD CONTACT AND MATERIALS AVAILABILITY

Further information and requests for resources and reagents should be directed to and will be fulfilled by the Lead Contact, Suwen Zhao (zhaosw@shanghaitech.edu.cn). This study did not generate new unique reagents.

EXPERIMENTAL MODEL AND SUBJECT DETAILS

Cell lines

Spodoptera frugiperda (Sf9) cells were used for α_{2A}AR expression and crystallization. CHO-K1 cells (ATCC) were used for Split luciferase biosensor cAMP assay.

METHOD DETAILS

Protein Engineering for Structure Determination

The sequence of the human α_{2A}AR gene was synthesized by GenScript. The modified thermostabilized apocytochrome b_{562}RIL (BRIL) was inserted into the receptor's third intracellular loop (IL3) at Thr227 and Arg365 of the human α_{2A}AR gene as a fusion partner, by overlapping PCR. The construct was further optimized by truncation of N-terminal residues 1-19 and C-terminal residues 446-450. The ΔN-α_{2A}AR-RS-BRIL-ΔC DNA sequence was subcloned into a modified mammalian expression pTT5 vector, which contained a haemagglutinin (HA) signal sequence, a FLAG tag and 10 × His tag, followed by a tobacco etch virus (TEV) protease cleavage site, before the N terminus of the truncated α_{2A}AR-RS gene. The ΔN-α_{2A}AR-RES-BRIL-ΔC DNA sequence was subcloned into a modified pFastBac1 vector for expression in Spodoptera frugiperda (*Sf9*) cells. The chimera sequence has a haemagglutinin (HA) signal sequence followed by a FLAG tag at the N terminus, a PreScission protease site and a 10 × His tag at the C terminus. Two rationally designed mutations, I121$^{3.40}$A and V122$^{3.41}$W, and three mutations, I121$^{3.40}$A, V122$^{3.41}$W, and I155$^{4.47}$L, were further introduced into the α_{2A}AR-RES and α_{2A}AR-RS genes, respectively, by standard QuickChange PCR.

Protein Expression

α_{2A}AR-RS construct was transfected and expressed in HEK293F cells (Invitrogen) (Passage number is 12-20) using the FreeStyle TM293 Expression system (Invitrogen). HEK293F cells (Invitrogen) were cultured in suspension starting from densities of 0.2-0.3 × 10^6 cells/ml in a humidified incubator with 5% CO_2 at 37°C with a shaking speed of 130 rpm. Passage cells when cell density reached 1.6-1.8 × 10^6 cells/ml. Briefly, HEK293F cells were seeded on day 0 at 6 × 10^5 cells/ml in freeStyle 293 expression medium (Invitrogen). On day 2 the transduction was performed at a cell density of 1.0 to 1.2 × 10^6 cells/ml and cell viability over 95% using PEI-DNA complexes. Approximately 48 h post-transfection, cells were harvested by centrifugation at 400 g for 20 min at 4°C. Cells were stored at −80°C for future use.

The α_{2A}AR-RES construct was transfected and expressed in *Sf9* cells. The Bac-to-Bac Baculovirus Expression System (Invitrogen) was used to generate high-titer recombinant baculovirus (> 109 viral particles per ml). Recombinant baculovirus was produced by transfecting recombinant bacmids (2.5-5 mg) into *Sf9* cells (2.5 mL, density of 106 cells/ml) using 5 mL of X-tremeGENE HP DNA Transfection Reagent (Roche) and Transfection Medium (Expression Systems). After 4 d of shaking at 27°C, P0 viral stock (~10^9 virus particles/ ml) was harvested as the supernatant of the cell suspension to produce high-titer viral stock. Viral titers were analyzed by flow cytometry on cells stained with gp64-PE antibody (Expression Systems). α_{2A}AR-RES was expressed by infecting *Sf9* cells at a cell density of 2-3 × 10^6 cells/ml with P1 virus at MOI (multiplicity of infection) of 5. Cells were harvested by centrifugation for 48 h post infection and stored at −80°C for future use.

Protein Purification

Frozen cell pellets were thawed and lysed by repeated washing and centrifugation in the hypotonic buffer of 10 mM HEPES (pH 7.5), 10 mM MgCl2, 20 mM KCl, and the high osmotic buffer of 10mM HEPES (pH 7.5), 1.0 M NaCl, 10mM MgCl2, and 20 mM KCl, with EDTA free complete protease inhibitor cocktail tablets (Roche). The washed membranes were suspended in hypotonic buffer with 30% glycerol and flash-frozen with liquid nitrogen and stored at −80°C until further use. Purified membranes were thawed at room temperature and incubated with 50 μM RES or RS 79948 and inhibitor cocktail at 4°C for 3 h. The membranes were further incubated with 1.0 mg/ml iodoacetamide (Sigma) for 1 h. The membranes were solubilized in the buffer containing 50 mM HEPES (pH 7.5), 200 mM NaCl, 1% (w/v) n-dodecyl-beta-D-maltopyranoside (DDM, Anatrace), and 0.2% (w/v) cholesterol hemisucinate (CHS, Sigma-Aldrich) at 4°C for 2.5-3 h. The supernatants containing the solubilized α_{2A}AR proteins were isolated by high-speed centrifugation, and then incubated with TALON IMAC resin (Clontech) and 20 mM imidazole, at 4°C overnight. The resin was washed with 15 column volumes of washing buffer I containing 25 mM HEPES (pH 7.5), 500 mM NaCl, 10% (v/v) glycerol, 0.05% (w/v) DDM, 0.01% (w/v) CHS, 30 mM imidazole, and 50 μM RES or RS, and then 5 column volumes of washing buffer II containing 25 mM HEPES (pH 7.5), 500 mM NaCl, 10% (v/v) glycerol, 0.05% (w/v) DDM, 0.01% (w/v) CHS, 50 mM imidazole, and 50 μM RES or RS 79948. The protein was eluted using 2.5 column volumes of elution buffer containing 25 mM HEPES (pH 7.5), 500 mM NaCl, 10% (v/v) glycerol, 0.01% (w/v) DDM, 0.002% (w/v) CHS, 250 mM imidazole, and 50 μM RES or RS 79948. A PD MiniTrap G-25 column (GE Healthcare) was used to remove imidazole. The protein was treated overnight with TEV protease to cleave the N-terminal FLAG/His tags from the proteins.

Lipidic Cubic Phase Crystallization

The purified α_{2A}AR protein in complex with RES or RS 79948 was screened for crystallization in lipidic cubic phase (LCP) with mixed molten lipid (90% (w/v) monoolein and 10% (w/v) cholesterol) at a protein/lipid ratio of 2:3 (v/v) using a mechanical syringe mixer (crystallizing membrane proteins using lipidic mesophases). LCP crystallization trials were set up using an NT8-LCP crystallization robot (Formulatrix). 96-well glass sandwich plates were incubated at 20°C in an automatic incubator/imager (RockImager 1000, Formulatrix) and imaged. Crystals were obtained in condition of 0.1M HEPES sodium pH 7.4, 310mM Ammonium tartrate dibasic, 36.5% PEG400 (RES) and condition of 0.1M Sodium citrate tribasic dihydrate pH 5.0, 290mM Ammonium chloride, 30% PEG400, 7% glycerol (RS 79948) and grew to full size in around two weeks. The crystals were harvested using micromounts (MiTeGen) and flash-frozen in liquid nitrogen.

Data Collection and Structure Determination

X-ray diffraction data of α_{2A}AR-RES and α_{2A}AR-RS crystals were collected at beam line 41XU at SPring-8, Japan, using a Pilatus3 6M detector. The data collection strategy was designed based on rastering results as previously described (Cherezov et al., 2009). Diffraction images were indexed, integrated and scaled using XDS (Kabsch, 2010) and merged using SCALA (Collaborative Computational Project, Number 4, 1994). Initial phases were obtained by the molecular replacement (MR) method with Phaser[4] using the receptor and BRIL portions of turkey β_1AR (PDB entry: 2Y02) as independent search models. Refinement was carried out with Phenix (Adams et al., 2010) and Buster (Smart et al., 2012) alternately followed by manual examination and adjustments of the refined structures in the program COOT (Emsley et al., 2010) with both 2|*Fo*|-|*Fc*| and |*Fo*|-|*Fc*| maps. In the final refined 2|*Fo*|-|*Fc*| maps, most of the 7TM structure and BRIL were ordered in both structures. The relatively high average B-factor of both structures (α_{2A}AR-RS complex:124.9; α_{2A}AR-RES complex: 160.4) may have been due to the particular molecule packing in crystals (Figure S2) with weak contact among transmembrane domain and strong contact among BRILs.

Cell culture and transfection for cAMP assay

To determine GPCR mediated cAMP production, we use Promega's split luciferase based GloSensor cAMP biosensor technology. CHO-K1 cells (ATCC), were maintained in F-12 supplemented with 10% FBS 1% penicillin/streptavidin. When cells reached 70% confluency in a 10 cm dish, 1 μg of target receptor DNA and 1 μg of GloSensor cAMP DNA were co-transfected by TransIT 2020(Mirus bio). On the following day, cells were seeded into 384-well white clear bottom cell culture plates (Greiner) at a density of 10-15,000 cells in 40 μL growth medium per well. To selectively ablate receptor- Gi coupling, 125 ng/mL pertussis toxin (PTX, Tocris) was added 18 hours before assay. The plates could be used for assays the next day.

Split luciferase biosensor cAMP assay

After removing supernatant from 384 well plates, wells were loaded for 60 min at 37°C with 20 μL of 2 mg/ml Luciferin prepared in HBSS with 0.1% BSA, pH 7.4. All the following steps were carried out at room temperature. To measure agonist activity on α_{2A}, 10 μL 4 × test drug solution was added for 15 min before the addition of 10 μL of forskolin (Sigma Aldrich) at a final concentration of 20 μM, followed by counting of the plate for chemiluminescence after 15 minutes. To measure antagonist activity, cells were preincubated with test drug for 15 min before 4 × 350 nM of UK14,304 and forskolin at a final concentration of 20 μM was added. Counting was undertaken after 15 min. Chemiluminescence signal was measured on an EnVision plate reader (Perkin Elmer).

Ligand docking

The whole process was done in Schrodinger Suite 2018-3. RES-bond and RS 79948-bond structures were prepared by Protein Preparation Wizard. Fusion partners were deleted, proteins were capped, and missing side chains were added. Protonation states were assigned by PROPKA. The directions of polar hydrogens were optimized and the whole structures were minimized. Grids were generated via Receptor Grid Generation in Glide (Friesner et al., 2004, 2006), hydroxyols in residues at positions 6.55, 5.42 and 5.46 were allowed to rotate during docking; RES or RS 79948 were select to define the center of the grid box. Ligands docked were downloaded from IUPHAR. LigPrep was used to prepare ligands so they will be ready to be docked. Epik was used to determine ligand's ionization states at pH 7.0 ± 2.0. Glide XP was used to dock ligands into two structures. After getting the result, those poses do not have a salt bridge between ligand and the residue at 3.32 were dropped.

QUANTIFICATION AND STATISTICAL ANALYSIS

The data obtained for individual experimental pEC_{50} between WT and mutated α_{2A}AR, WT β_2AR presented as the mean ± SEM ($N \geq 3$) in Prism 7 (GraphPad, La Jolla, CA).

DATA AND CODE AVAILABILITY

The accession numbers for the structures of α_{2A}AR-RS 79948 complex and α2AAR-RES complex reported in this paper are PDB: 6KUX and 6KUY, respectively. All other data are available from the corresponding authors upon request.